CONSTRUCTION OF AN ELECTRON PARAMAGNETIC RESONANCE SPECTROMETER

George Russell Sharp

A THESIS

in

The Department

of

Physics

Presented in Partial Fulfillment of the Requirements
for the Degree of Master of Science at
Sir George Williams University
Montreal, Canada

September, 1972

ABSTRACT

The details of construction of an X-band paramagnetic resonance spectrometer and its operation are presented. Particular attention is focused on the automatic frequency control unit for the klystron and the low temperature cryostat suitable for measurements at liquid helium temperatures, which were assembled in this laboratory.

As a demonstration of satisfactory performance of the spectrometer, electron paramagnetic resonance spectra of chromium potassium alum ($CrK(SO_4)_2 \cdot 12H_2O$) and the free radical diphenyl pycryl hydrazl (d.p.p.h.) are presented. The results show satisfactory agreement with published data.

TABLE OF CONTENTS

ACKNOWLEDGEMENTS

The author wishes to express gratitude to Dr. S.K. Misra for proposing this work and for his continued interest and advice. He gratefully acknowledges the encouragement received from his father and Dr. B. Frank. He is also indebted to Mr. J. Blaison, Mr. A. Christodoulopoulos and Mr. J. Loustau for their very helpful technical assistance.

The financial assistance provided by Dr. S.K. Misra from his N.R.C. grant and by the Physics Department are gratefully appreciated.

CHAPTER I

INTRODUCTION

The evolution of electron spin resonance begins with the discovery of the phenomena by Zavoisky[1] in 1945. He observed strong paramagnetic resonance absorptions in several salts. Other early contributors to the field were Bleaney and Penrose[2]. In the past twenty-five years this field has grown tremendously and has been the subject of a large number of publications.

This thesis is concerned with the instrumentation part of the project involving the detection of dynamically oriented nuclei by the Mössbauer effect.[3,4] Thus it was not the intention to build a highly sensitive spectrometer, but one that is satisfactory for dynamic nuclear orientation at X-band frequencies, requiring the use of liquid helium temperatures. For this reason a homodyne system using a magic tee as the bridge element has been built.

In chapter II the theory of paramagnetic resonance is briefly presented. The details of the e.p.r. spectrometer assembly are given in chapter III. Chapter IV describes the construction of the low temperature cryostat and the measurement and control of the temperature. Plotting of the absorption spectra of chromium

potassium sulfate ($CrK(SO_4)_2 \cdot 12H_2O$) and the free radical diphenyl picryl hydrazl (d.p.p.h.) and related discussion form the subject of chapter V.

CHAPTER II

THEORY

A paramagnetic substance may be defined as one that possesses no resultant magnetic moment in the absence of an external field but acquires a magnetic moment in the direction of an applied field whose size is a function of the field. For the free electron, quantum theory stipulates that only two values of energy are permitted, which means that the electron spin can only assume two orientations relative to the applied magnetic field.

An important class of paramagnetic substances are those where the constituent atoms (or ions) have permanent magnetic moments. In the absence of an external field such dipoles are randomly oriented, but the application of a magnetic field results in redistribution over the various orientations in such a way that the substance acquires a net magnetic moment.

When a strong magnetic field H is applied to the electron, the electron experiences a torque acting on it in such a way to make it precess with a frequency which is proportional to the applied magnetic field and the magnetic moment. The frequency of precession about H is called the Larmor frequency and its value is given by the

relation

$$\omega = -\gamma H \tag{1}$$

where γ is the magnetogyric ratio, $-g(e/2mc)$ for the electron. Since γ is positive the precession is in the direction of a right-hand screw advancing along H as shown in Fig. 1.

In addition to a strong magnetic field H, a rotating magnetic field H_1 of frequency ν may be applied perpendicular to H. This furnishes a phase reference for all similar electrons in the sample resulting in the phenomenon of induction and a secular torque is exerted on each of the electrons tending to tip its moment relative to the strong field H.

Stimulated absorption occurs when the value of H is such that the microwave frequency is equal to the Larmor frequency. A photon of energy $h\nu$ is then absorbed from the radiation field accompanied by a spin transition from $M_s = -1/2$ to $M_s = +1/2$. The condition for resonance can thus be written as

$$\hbar\omega = h\nu = g\beta H \tag{2}$$

where β is the Bohr magneton (the magnetic moment of the electron) given by $eh/2mc$.

Figure 2 shows an energy level diagram for the case of spin 1/2 free electrons in an external magnetic field H. At the right are the two possible orientations designated by the quantum numbers +1/2 and -1/2; N^+ and N^- are the electron populations in the two levels +1/2 and -1/2 respectively; $g\beta H$ is the energy difference of the Zeeman splitting; and W_e and W_a are the respective absorption and emission probabilities. In general for any pair of energy levels the spin populations will be inversely proportional to the transition probabilities given by

$$N^-/N^+ = W_e/W_a = \exp(\epsilon/kT) \tag{3}$$

where $\epsilon = g\beta H$. This leads to the fact that for a detectable absorption or emission, a non-zero difference in the spin population of the two energy levels, that is $N^- \neq N^+$, is required. Also the relation shows that by lowering the temperature, the N^-/N^+ ratio is enhanced and thus the detectable signal.

2.1 The Spin Hamiltonian

Most of the cases of interest for example paramagnetic crystals, the electron is not free but it interacts with the nuclei and electrons of the sample in varying degrees so the energy absorbed is not only a function of the Zeeman interaction but of numerous other components. The electronic interactions which contribute to the total

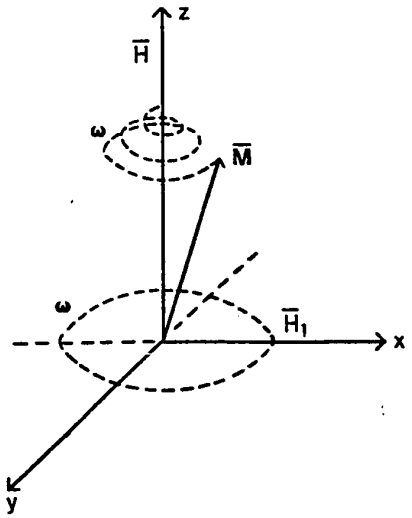

Fig. 1 Precessing electron moment

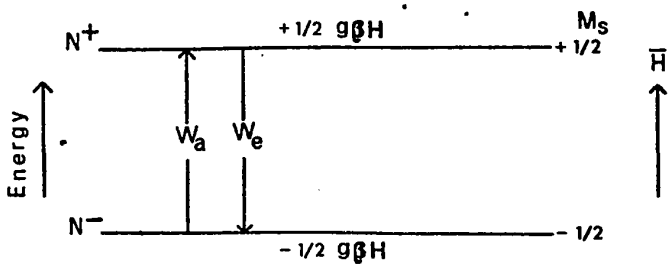

Fig. 2 Energy level diagram for simple spin 1/2 system of free electrons

energy of the ion can be represented by the following Hamiltonian.[5]

$$\mathcal{H} = \mathcal{H}_{elect} + \mathcal{H}_{cf} + \mathcal{H}_{LS} + \mathcal{H}_{SS} + \mathcal{H}_{Zee} + \mathcal{H}_{hfs} + \mathcal{H}_{Q} + \mathcal{H}_{N}$$

Table 1 gives the typical form of each term and their magnitudes.

Since the energy contribution from the various terms ranges over nine decades some of the interactions fall out of the realm of electron spin resonance. The terms $\mathcal{H}_{elect}$, $\mathcal{H}_{cf}$, and $\mathcal{H}_{LS}$ involve too much energy for excitation and the terms $\mathcal{H}_{Q}$ and $\mathcal{H}_{N}$ are too small to be observed in most cases. Other terms or portions of terms can be eliminated when the composition and crystal structure is known.

2.2 Relaxation Times

The line width of absorption lines is determined to a large extent by two relaxation processes; spin-lattice relaxation and spin-spin relaxation.

The spin-lattice relaxation time T_1 transfers energy from the spin system to the lattice by the direct or Raman process. In the direct process the spins can transfer energy to a lattice vibration which has essentially the same frequency. The value of T_1 for the

Table 1 The various terms of the spin Hamiltonian

$\mathcal{H}_{elect}$ = electronic energy = 10^4-10^5 cm^{-1} (optical region)

$\mathcal{H}_{cf}$ = crystal field energy = 10^3 - 10^4 cm^{-1} (infrared or optical region)

$\mathcal{H}_{LS}$ = spin orbit interaction = 10^2 cm^{-1} $= \lambda \bar{L} \cdot \bar{S}$

$\mathcal{H}_{SS}$ = spin-spin interaction = 0-1 cm^{-1} $= D(S_z^2 - 1/3S(S+1))$

$\mathcal{H}_{Zee}$ = Zeeman energy = 0-1 cm^{-1} $= (\bar{H} \cdot \bar{\bar{g}} \cdot \bar{S})$

$\mathcal{H}_{hfs}$ = Hyperfine structure = 0-10^{-2} cm^{-1} $= (\bar{S} \cdot \bar{\bar{A}} \cdot \bar{I})$

$\mathcal{H}_Q$ = Quadrupole energy = 0-10^{-2} cm^{-1} = $\{3eQ/[4I(2I-1)]\} \times \partial^2 V/\partial z^2 [I_z^2 - (1/3)I(I+1)]$

$\mathcal{H}_N$ = nuclear spin energy = 0-10^{-3} cm^{-1} $= (\bar{H} \cdot \bar{I}) \gamma \beta_n$

The symbols are defined as follows:

λ = spin orbit coupling constant

S = electronic spin

L = orbital quantum number

D = zero field splitting constant

β = Bohr magneton

A = hyperfine coupling constant

I = nuclear spin

e = electronic charge

Q = nuclear electric quadrupole moment

V = crystalline electric field potential

γ = nuclear magnetogyric ratio

β_n = nuclear magneton

direct process is proportional to $1/H^2T$ where T is the temperature. The direct process is independent of spin concentration and occurs only at temperatures below 4°K. The Raman process is predominate at high temperatures. The spins in this process transfer energy by scattering a quantum from the lattice in the process of flipping its spin. The value of T_1 is proportional to $1/T^2$ for this process.

The spin-spin interaction causes broadening due to the mutual interactions of magnetic dipoles. The magnetic dipoles which precess in the applied magnetic field have a steady component in the direction of the field. This component acts on the neighbouring ions and causes local disturbances over the entire spin system which shifts the energy values. The interactions depend on the precessional frequency of the neighbouring dipoles and their concentration. Since dipole-dipole interaction is inversely proportional to the cube of the separation of the dipoles many interactions can be eliminated by diluting the environment with diamagnetic atoms.

2.3. Exchange Interaction

In many paramagnetic compounds the separation of the magnetic ions is less than about 0.5×10^{-9} m^6 and exchange interaction between neighbours exceeds the effect of dipole-dipole interaction. If the spins are similar the effect is to narrow the lines at the center and broaden them in the wings. The width at half maximum intensity is

reduced therefore the phenomenon is known as "exchange narrowing". If the exchange of spins is between two dissimilar ions the exchange interaction will bring two different transitions together and hence produce a single wide line.

A useful and striking example of exchange narrowing is the paramagnetic organic crystal d.p.p.h. or the "g marker".[7] This free radical has a 1.35 gauss half-width of the resonance line at half power, which is only a few percent of the pure dipolar width.

CHAPTER III

THE PARAMAGNETIC RESONANCE SPECTROMETER

A reflection cavity X-band spectrometer[8] suitable for dynamic nuclear orientation was assembled. A block diagram of the spectrometer is shown in Fig. 3. The description of the various components is as follows. The automatic frequency control unit has been described in detail since it was assembled in the laboratory.

3.1. The Microwave Source

The microwave source is a forced air cooled Varian X-13 reflex klystron with a frequency range of 8.1 to 12.4 gHz and a power rating of 180 mw. A Hewlett Packard model 715A power supply produces the required beam voltage of +400 vdc with a ripple of less than 7 mv and a beam current of 50 ma. A wide range of reflector voltages from 0 to -900 vdc with respect to the beam supply are available with a ripple of less than 10 mv. The filament voltage supply provides 1.5 amps at 6.3 vac.

A 0 to 350 vac peak to peak sinusoidal signal is available to display the modes of the klystron as shown in Fig. 4.

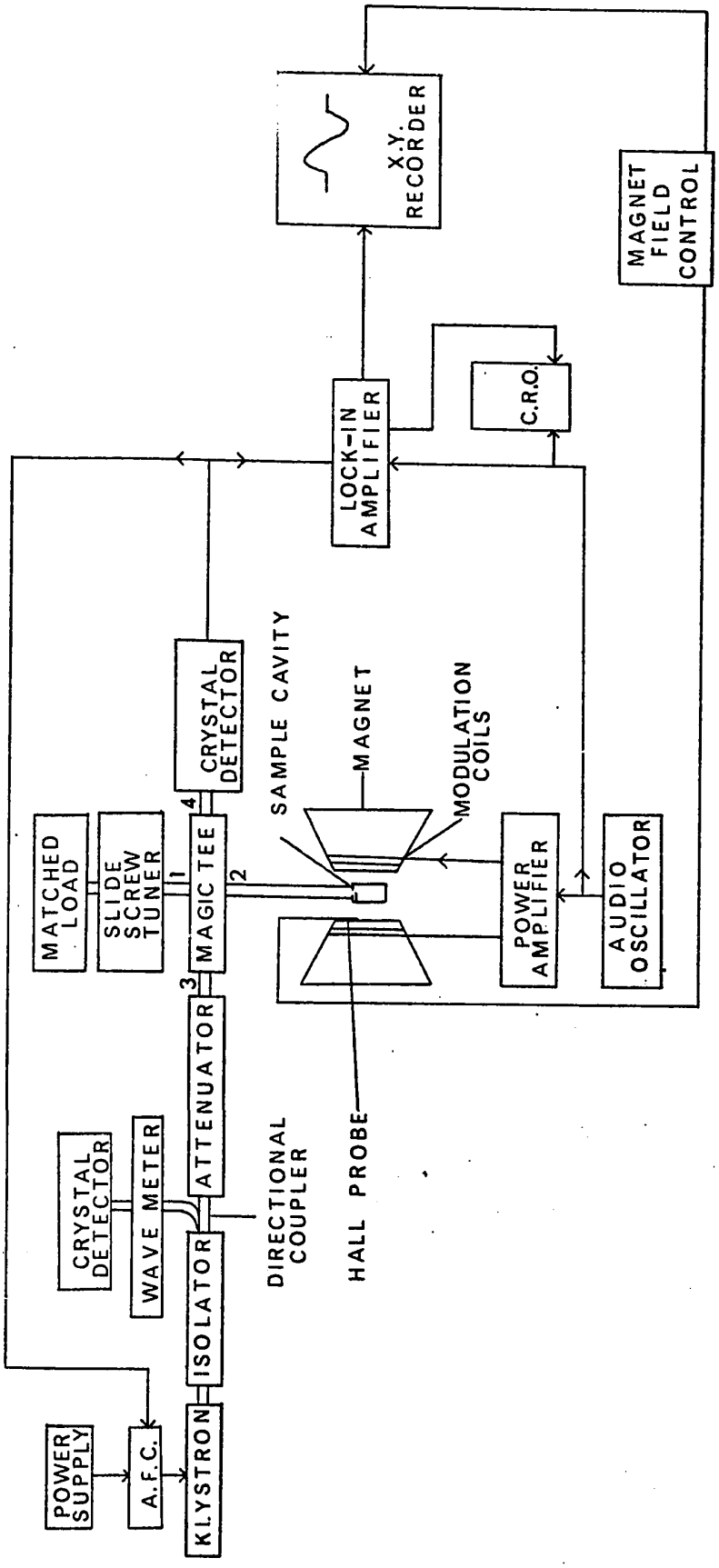

Fig. 3. Block diagram of the X-band spectrometer

3.2 The Waveguide Network

The DeMornay-Bonardi model DBG-480 isolater permits the transmission of microwaves in one direction and prevents their transmission in the opposite direction. This prevents the waveguide network from acting back on and influencing the frequency stability of the klystron.

In order to measure the frequency of operation ten percent of the microwave power is coupled off to a Hewlett Packard model 532 frequency meter with a dial accuracy of 0.05 percent. The microwave power is detected by a Hewlett Packard model X424A crystal detector. The resonance frequency is indicated on the scope when a dip in the transmitted power is observed.

A Hewlett Packard model 382 calibrated attenuator is between the load and the generator to reduce the signal intensity incident upon the load. This is adjusted to give optimum signal to noise ratio. At room temperature due to fast relaxation times, the saturation of spin transitions is no problem thus little or no attenuation is needed to observe a signal. However at lower temperatures, lesser power should be used to observe the resonance absorption since saturation occurs easily due to long relaxation times.

The required power from the attenuator enters arm 3 of the DeMornay-Bonardi model DBG-650 magic tee where the power splits between arms 1 and 2. Arm 2 is the cavity arm which will be discussed in section 3.3. Arm 1 is made up of a Hewlett Packard model 870A slide screw tuner and a Hewlett model 914B matched load. The slide screw tuner is used to produce an under coupled cavity match because the crystal detector operates more efficiently with a finite amount of power incident upon it at all times. The longitudinal position is varied until one obtains maximum leakage as shown in Fig. 5 on the crystal detector and its insertion is adjusted for about ten percent of the power incident upon the cavity. Arm 4 is the detector arm to which is connected a Hewlett Packard model 485B detector mount containing a 1N23D silicon diode which provides a good signal to noise ratio.

3.3 The Sample Cavity

Figure 6 shows a detailed view of the cavity arm of the spectrometer. This arm has been designed for use inside the cryostat thus the top flange is sealed off for evacuation purposes by means of a mica sheet and silicone cement on the outside. The cavity arm is evacuated so as to reduce condensation and thus preserve tuning of the cavity at low temperatures.

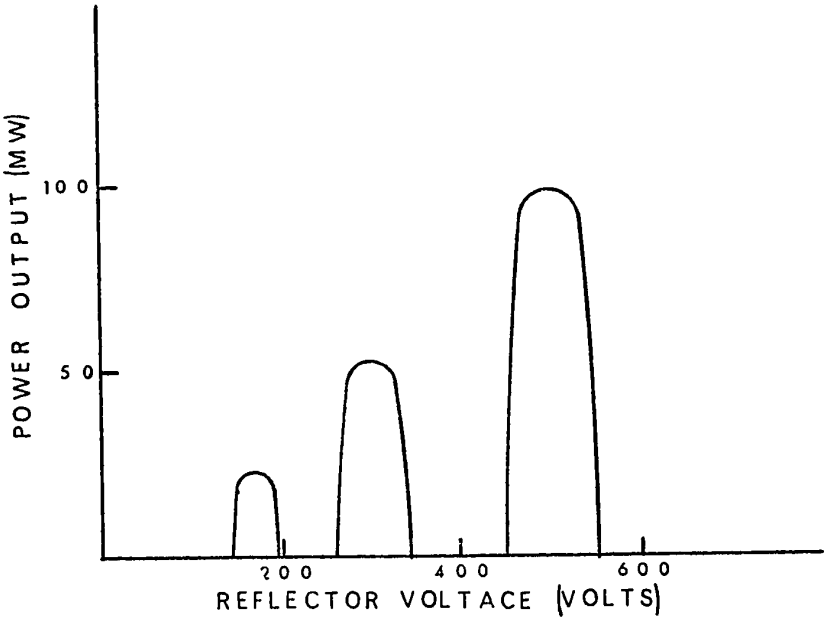

Fig. 4 Klystron modes

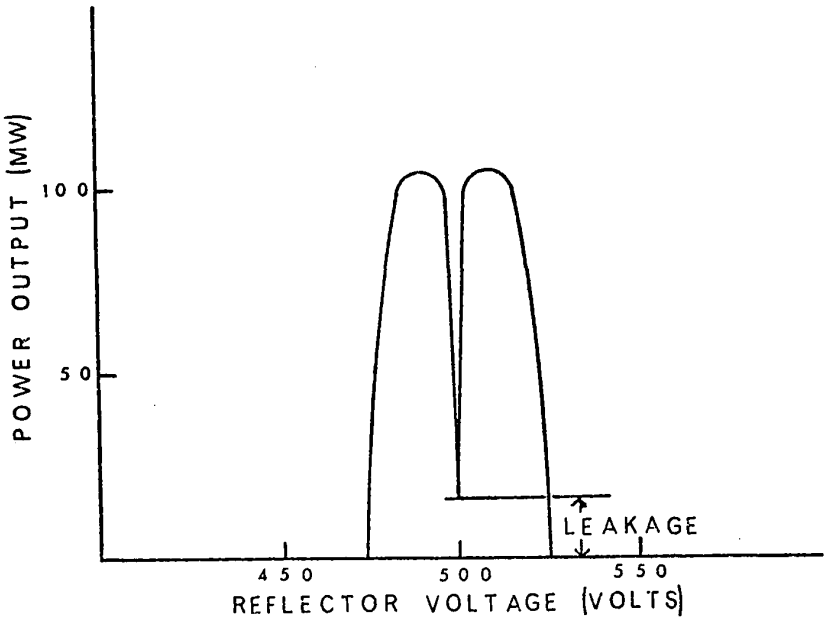

Fig. 5 Klystron mode with cavity frequency centered on mode

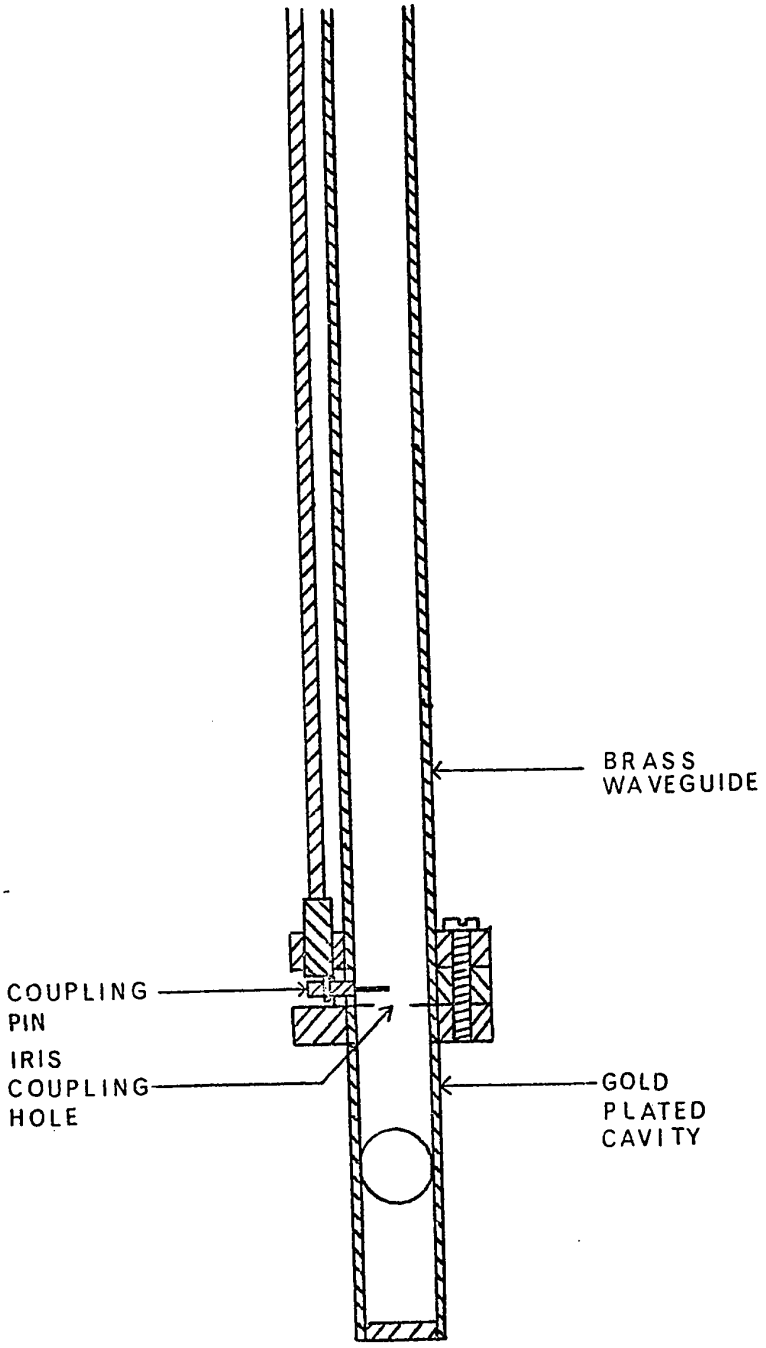

Fig. 6 Detailed view of cavity arm

The cavity, which is gold plated, is a rectangular type, resonating in the TE_{102} mode at a frequency of 9.46 gHz to wavemeter accuracy. The generalized relationship for the wavelength[9] in a uniform rectangular waveguide operating in the TE_{10n} mode is

$$1/\lambda_g^2 = 1/\lambda_0^2 + 1/\lambda_c^2 \qquad (4)$$

where λ_g = guide wavelength

λ_0 = free space wavelength

λ_c = cutoff wavelength

λ_c = 2a, where a is the broad dimension of the rectangle

Also $\lambda_0 = c/f_o$

Substituting gives

$$\lambda_g = \frac{29.97925}{f_o\sqrt{1-\left(\frac{29.97925}{f_o 2a}\right)^2}} \qquad (5)$$

For a resonant frequency of 9.50 gHz the guide wavelength turns out to be 4.361 cm. Due to a difference of .54 mm after machining and gold plating the resonant frequency of the cavity is 9.46 gHz.

The cavity was built in the workshop and was equipped with 3/8 inch holes in b sides (the narrow dimension of the waveguide) to allow for irradiation of the sample with gamma rays required for the Mossbauer effect detection of dynamically oriented nuclei. Results using this cavity with holes showed that the amplitude of the resonance absorption curve was attenuated by approximately

five percent compared to that obtained with no holes.

The cavity is coupled to the waveguide by a 0.010 inch gold plated brass sheet with an iris in the center of 0.20 inch diameter.[10] The cavity is matched to the waveguide by a 0.030 inch inductive pin. The pin is connected to a cam and rod which leads to the upper flange of the cryostat. The arrangement was necessitated by the fact that the resonant frequency and the coupling of the cavity are temperature sensitive and one must be able to adjust externally at low temperatures.

The cavity, iris and mounting for the tuner are connected to a flange at the end of a ten inch brass waveguide by four machine screws. The brass waveguide is chosen in order to add weight to reduce cavity vibrations. The brass waveguide is hard soldered to a 0.020 inch wall stainless steel waveguide which leads to the top of the cryostat. This serves to insulate the cavity as much as possible from room temperature.

3.4 The Automatic Frequency Control

The circuit of the automatic frequency control unit assembled is shown in Figs. 7(a) and 7(b).[11] A Hewlett Packard model 204C

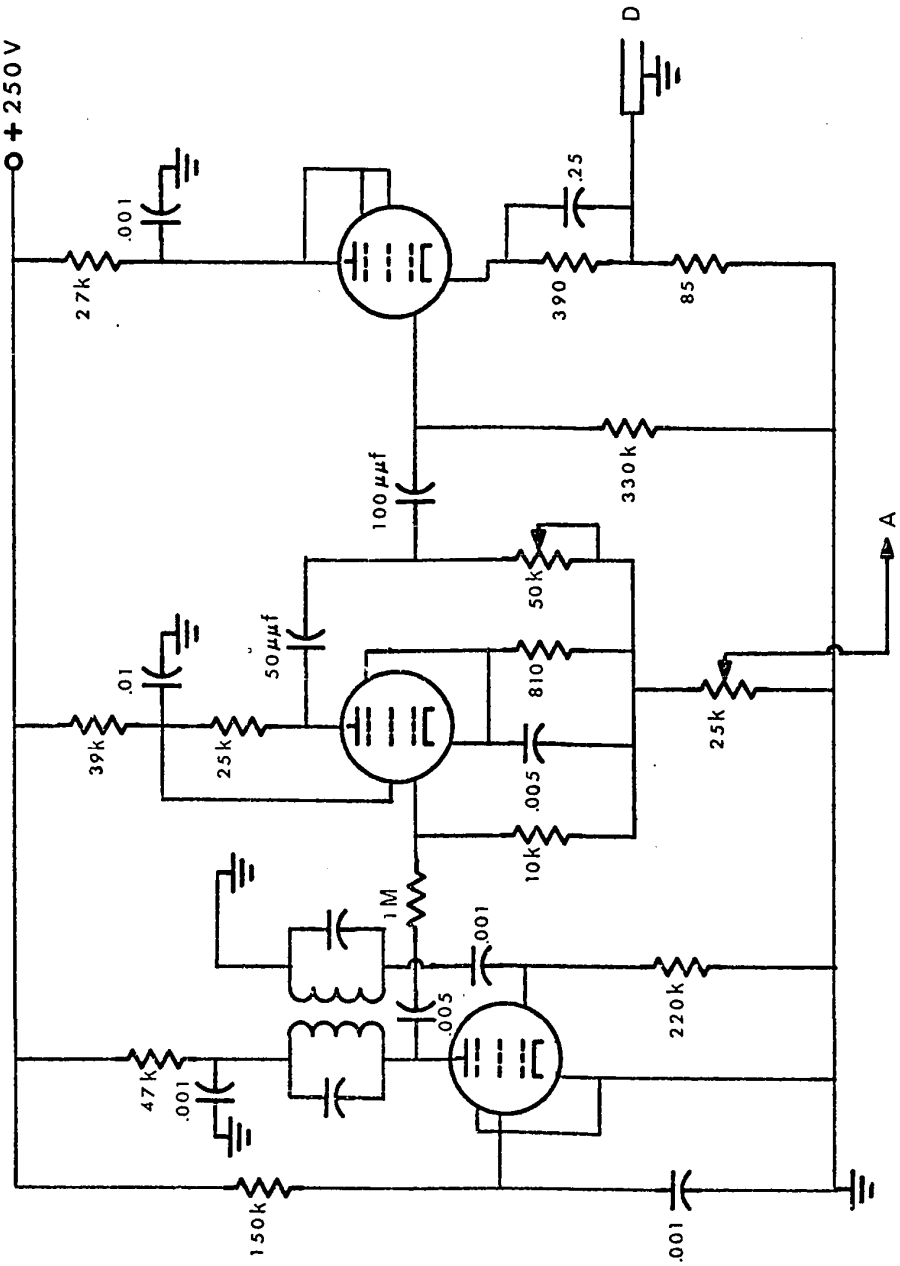

Fig. 7(a) Oscillator and modulation feed circuit

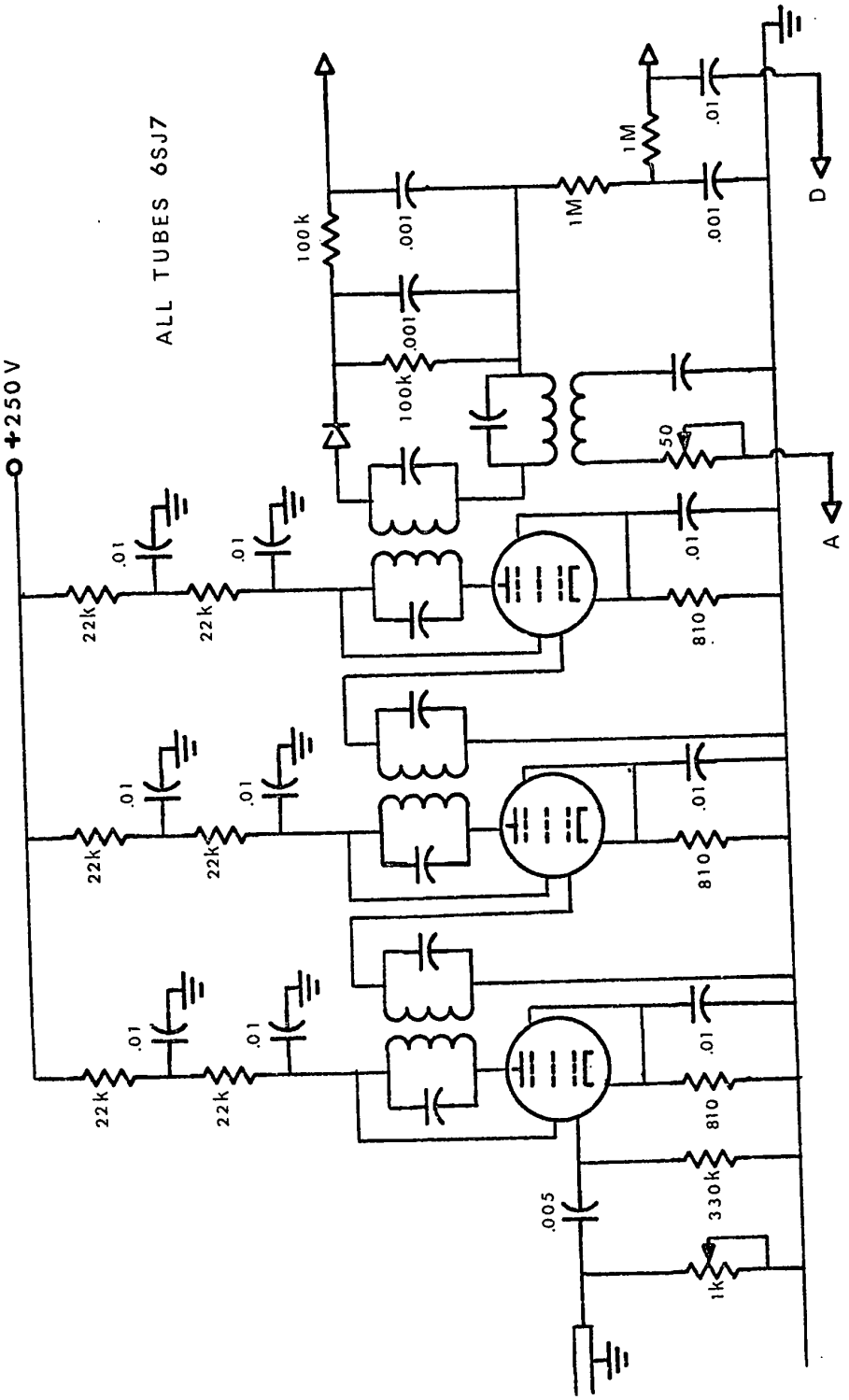

Fig. 7(b) Amplifier and phase sensitive detector circuit

oscillator is used to supply a large modulation voltage to tune the microwave bridge. The automatic frequency control is either locked to the frequency of the frequency meter or the sample cavity. It is usually locked to the sample cavity so that if for any reason, such as temperature changes of the sample cavity, the klystron frequency will follow the change.

A control frequency of 465 kHz is provided by the oscillator to both the phase detector via an amplifier and a cathode follower and to the klystron reflector whose potential is of the order of -500 vdc. When the klystron center frequency (f_o) corresponds to the resonant frequency of the sample cavity (f_r) the second harmonic of the modulation frequency is reflected from the cavity and appears at the crystal detector as shown in Fig. 8(a). If the center frequency of the klystron is shifted from that of the resonant cavity, the frequency of the signal appearing at the crystal detector is 465 kHz. Its phase is dependent on whether the klystron center frequency is higher (Fig. 8(b)) or lower (Fig. 8(c)) than the resonant cavity frequency. The amplitude of the reflected 465 kHz signal is dependent upon the relative difference between f_o and f_r.

The voltage f_r is amplified by a three stage transformer coupled amplifier, each stage having a gain of one hundred. The

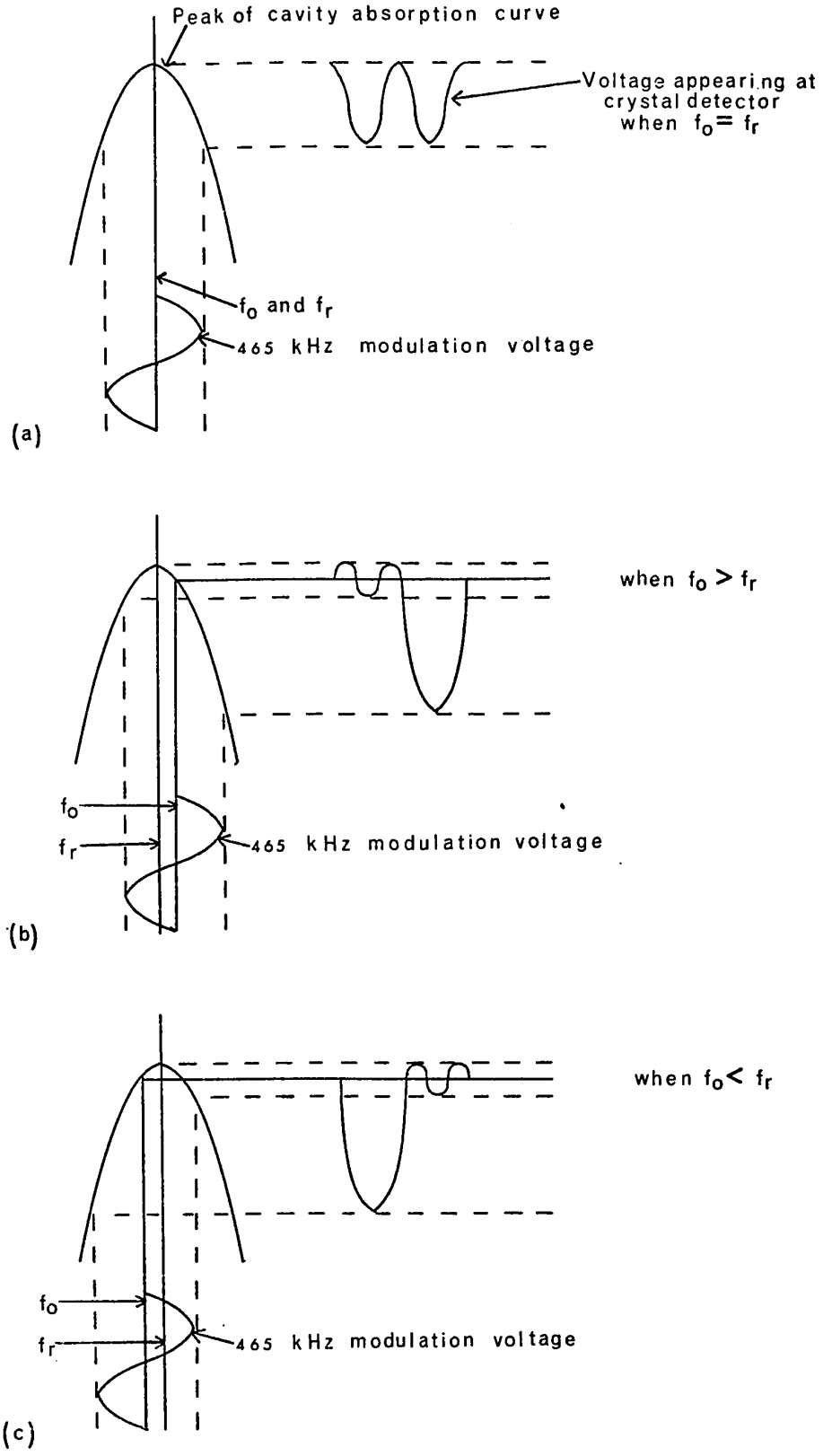

Fig. 8 Output voltages from cavity as a result of A.F.C. modulation

amplified signal and the 465 kHz reference signal enter the additive type phase sensitive detector. On the condition that the reference signal is larger than the amplified signal the detection will be phase sensitive. The resulting dc output voltage is applied to the klystron reflector so the center frequency of the klystron corresponds to the frequency of the resonant cavity.

Since it is essential that the electronic noise be at a minimum in an electron paramagnetic resonance spectrometer several precautions were taken in building the amplifier stage: all plate and control grid connections were made as short as possible, a brass rod connected at either end of the chasis was used as a common ground to reduce noise caused by ground loops, wires which had to cross each other were crossed at right angles to reduce stray capacitance and shielded cable was used on all signal carrying wires.

For domestic radio sets it is preferable to have the intermediate-frequency transformers slightly overcoupled thus producing a broader amplifier bandwidth. This overcoupling is caused by the mutual inductance between the windings on the core of the transformers. Since one requires slightly undercoupled intermediate frequency transformers to obtain a narrow response curve the coils were heated and pulled further apart.

3.5 The Detecting and Amplifying System

The crystal detector demodulates the microwave power which is then transferred by a coaxial cable to the Princeton Applied Research model 122 lock-in-amplifier. This instrument enables the rms value of the fundamental frequency component to be measured accurately.

The basic element of the amplifier is a phase sensitive detector in which the signal voltage is mixed with a reference voltage, producing sum and difference frequencies. A low pass filter at the output of the mixer rejects the high frequency components corresponding to the sum frequencies and passes the difference frequencies which lie in the frequency band which are allowed to pass. The difference frequencies from components of the signal spectrum which differ from the reference frequency by more than the cut-off frequency of the low pass filter are attenuated. Consequently the output of the low pass filter will be due to that portion of the signal spectrum which lies about the reference frequency within a pass-band determined by the low pass filter.

The front panel "monitor" switch allows either the output of the signal amplifier or the output of the reference tuned amplifier

or the output of the dc amplifier to appear at both the monitor jack for display and the meter. The sensitivity of the signal channel can be varied from 0.1 mv to 50.0 mv. The time constants can also be varied from 1 msec to 30 sec. A time constant of 1 sec gives the best signal to noise ratio as well as the derivative of the absorption curve.

The reference channel can be tuned over a frequency range of 5 Hz to 150 kHz by means of a continuous front panel control. There is a continuously adjustable phase shifter with a range of 0° to 315° phase shift as well.

The resulting dc output from the lock-in-amplifier is plotted on a Moseley model 7005A servo potentiometer X-Y recorder. Each axis of the recorder has an independent servo system with no interaction between channels. Each axis has five fixed calibrated ranges from 0.4 mv/cm to 4 v/cm. The X-axis is driven by a fraction of the signal provided by the "X-axis drive" of the Varian Fieldial which was used to regulate and sweep the magnetic field. The Y-axis is driven by the output of the lock-in-amplifier, thus yielding a plot of the derivative of absorption versus magnetic field.

3.6. Production of Magnetic Fields

The magnetic field H is provided by a Varian V-3900 electromagnet which is capable of producing a field of 13k G across a 3 inch magnet gap. The center of each pole piece contains a 0.50 inch hole for the purpose of irradiating samples when radiation is incident in the longitudinal position with respect to the magnetic field. The pole pieces are equipped with shims to produce a homogeneous field.

The Varian 10-kW VFR-2803 control unit has digital field control dials with increments of 0.10 G which assures accurate field settings. The control panel also includes a field reversing switch, a test selection switch, a meter to monitor the magnet system operation and a complete linear sweep. Sweep ranges from 0.25 G to 10k G with sweep times of 0.50 min to 100 min can be selected. A temperature controlled Hall-effect crystal probe mounted on one magnet pole cap maintains the magnetic field within one percent of the selected field value.

3.7. Magnetic Field Measurements

The digital field controls were calibrated by means of nuclear magnetic resonance probes containing protons for fields of

1 kG to 8 kG and deutrons from 8 kG to 10kG. This was done with the sweep off. The difference between the fieldial reading and the true field was found to be linear over the range 1 kG to 10 kG. The values were fit using a standard linear curve fit program. The magnetic fields are reproducible with respect to this calibration to less than 0.20 percent which is adequate for paramagnetic resonance experiments. A portion of the calibration is listed in Appendix A.

Nuclear magnetic resonance is a well known principle and commonly used to measure and calibrate magnetic fields. The resonance condition is $2\pi\nu=\gamma H$ where ν is the applied frequency, γ is the magnetogyric ratio of the nucleus and H is the applied field. For protons this becomes $H=0.23487\nu$ where H is given in gauss and ν in Hz. To determine the magnetic field by this method, the frequency at resonanceis measured, the accuracy in this measurement can easily be 1 part in 10^5.

The instrument used to make these measurements was a Varian F-8 nuclear fluxmeter and a Hewlett Packard model 5245N frequency counter. Neglecting the effect of an inhomogeneous magnetic field the possible error is .0038 percent which is constant throughout the range of the fluxmeter.

The sweep scales of the Fieldial were calibrated by using the g-marker (d.p.p.h.) at a single frequency (9.46 gHz to wavemeter accuracy). This was done to have a continual check of the calibration. The resonant field was found with the sweep set at 0% of the full scale under test. The sweep scale was then set to +50% and -50% of full scale and the resonance again found by resetting the digital field controls. The results are tabulated in table 2.

Table 2. Calibration of Fieldial sweep scales

Full Scale (gauss)	Sweep Dial Setting 0%	+50%	-50%	Δ max gauss
100	3395.4	3345.3 (3395.3)	3444.7 (3394.7)	0.7
250	3395.4	3271.3 (3396.3)	3520.3 (3395.3)	0.9
500	3395.2	3147.3 (3397.3)	3647.2 (3397.2)	2.1
1000	3393.8	2896.8 (3396.8)	3896.9 (3396.9)	3.1
2500	3393.4	2156.7 (3406.7)	4655.4 (3405.4)	13.3
5000	3393.8	913.0 (3413.0)	5915.4 (3415.4)	21.7

The results of table 2 indicate that the small sweep scales should be used for accurate field determination. In order to check the homogeneity of the field as well as the correct location of the sample cavity in the field, the resonant field of d.p.p.h. was found for a rotation of 180°. The field values were found to be within ± .52 G.

3.8 Magnetic Field Modulation

The magnetic field is modulated at a frequency of 390 Hz using a sinusoidal sweep small as compared to the dc magnetic field. The modulation amplitude is adjusted to give a good representation of the desired derivative. Too large a modulation causes the line to be broadened and distorted and too small a modulation causes the line to be buried in noise.

The pair of coils are wrapped on a masonite form and rigidly mounted on the magnet pole pieces. They are epoxied to reduce vibrations. Each coil is 90 turns of number 12 insulated copper wire. These were connected in series with a 30 μF capacitor to the power amplifier. A Hewlett Packard model 204C oscillator supplied the sinusoidal signal. The power amplifier is shown in Fig. 9. The amplifier is capable of producing 100 w rms, the maximum current being 7 amps ac rms.

At high fields (larger than 5 kG) and high modulation amplitude the coils were extremely noisy, although precautions were taken to avoid this as mentioned above. When any part of the apparatus touched the pole pieces the reception of the signals was perturbed by strong microphonics. It was therefore carefully avoided that the cryostat touched any part of the magnet.

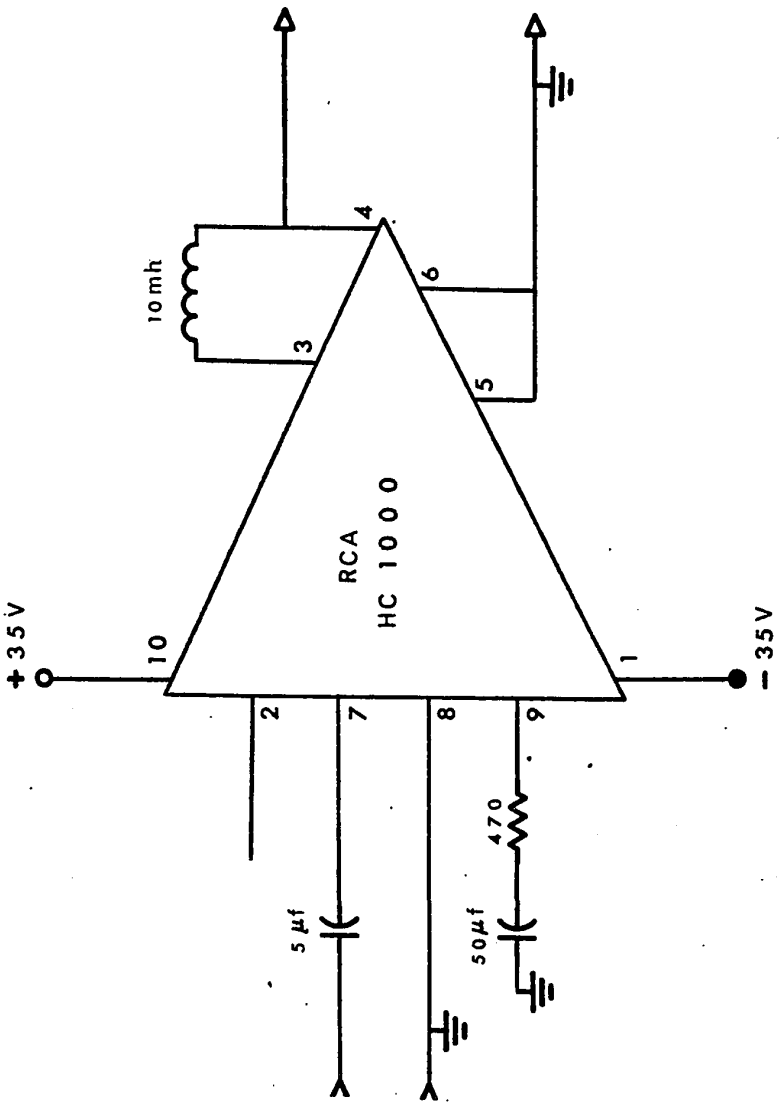

Fig. 9 Power Amplifier Circuit

3.9 Principle of Detection

The cavity is tuned so that all available power from the klystron is absorbed by the cavity when the resonance occurs at a given frequency, the frequency being dependent upon the dimension of the cavity. When the frequency of the microwave field and the amplitude of the magnetic field satisfy the resonance condition of the sample, the impedance of the cavity is changed and a signal is reflected to the crystal detector in the hybrid tee.

Figure 10 (a) represents the change in output at the detector as a simple function of the steady magnetic field at the sample, Fig. 10(b) shows the variation of the field as a function of time when the linear sweep and the sinusoidal field variations are applied, and Fig. 10(c) shows how the static curve translates these variations into a time varying signal at the output of the microwave detector. The signal at the output of the amplifier varies in time in the manner indicated in Fig. 10(d). The change in the sign of the derivative of the absorption curve is conveyed in the waveform of Fig. 10(d) as a reversal in phase relative to the field modulation waveform. The waveform at the output of the amplifier enters the phase sensitive detector that uses the original sinusoidal waveform as reference. The dc output of the detector is a representation of the derivative of the absorption line as shown in Fig. 10(e).

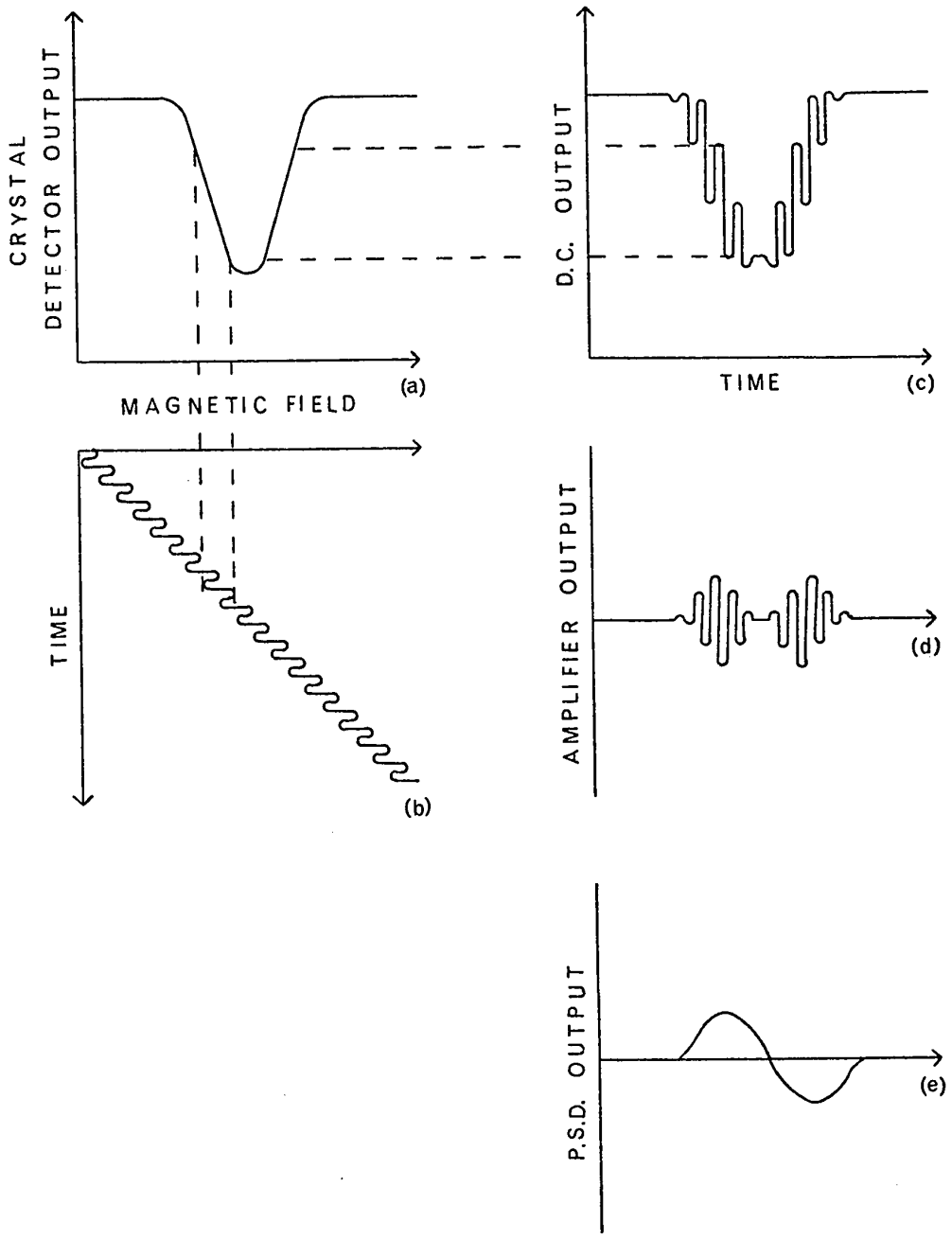

Fig. 10 Waveforms illustrating the operation of a spectrometer

CHAPTER I V

LOW TEMPERATURE APPARATUS

The liquid helium cryostat shown in Figs. 11(a) and 11(b) has been constructed to provide maximum versatility. The totally metallic construction is the same as many commercially available models. The decision to build the cryostat in the workship was prompted by the fact that we required changes in the commercially available models, the cost of these being very high. The changes allow for simultaneous electron spin resonance and Mossbauer effect experiments in a magnet air gap of 3.125 inches.

The cryostat body provides the working reservoir for the cryogenic fluids, the evacuation and the necessary mounting or support facilities for the entire assembly. All parts used, except where otherwise indicated, are made of non-magnetic stainless steel. Since polished stainless steel is not available in small quantities about 200 hours were spent in polishing the tubes with emery cloth. In order to insure a good vacuum all non-demountable joints were inert gas welded and then leak tested at room temperature and liquid nitrogen temperature.

A WAVEGUIDE
B ELECTRICAL CONNECTOR
C HELIUM VENT
D HELIUM PUMPING ARM
E NITROGEN VENT
F OUTER SHELL
G NITROGEN RESERVOIR
H HELIUM RESERVOIR
I INSULATION SPACE
J OUTER TAIL
K RADIATION SHIELD
L INNER TAIL
M BERYLLIUM WINDOWS
N CAPPILLARY TUBE
O THROTTLE VALVE
P THROTTLE VALVE STEM
Q NITROGEN FILL
R THROTTLE CONTROL

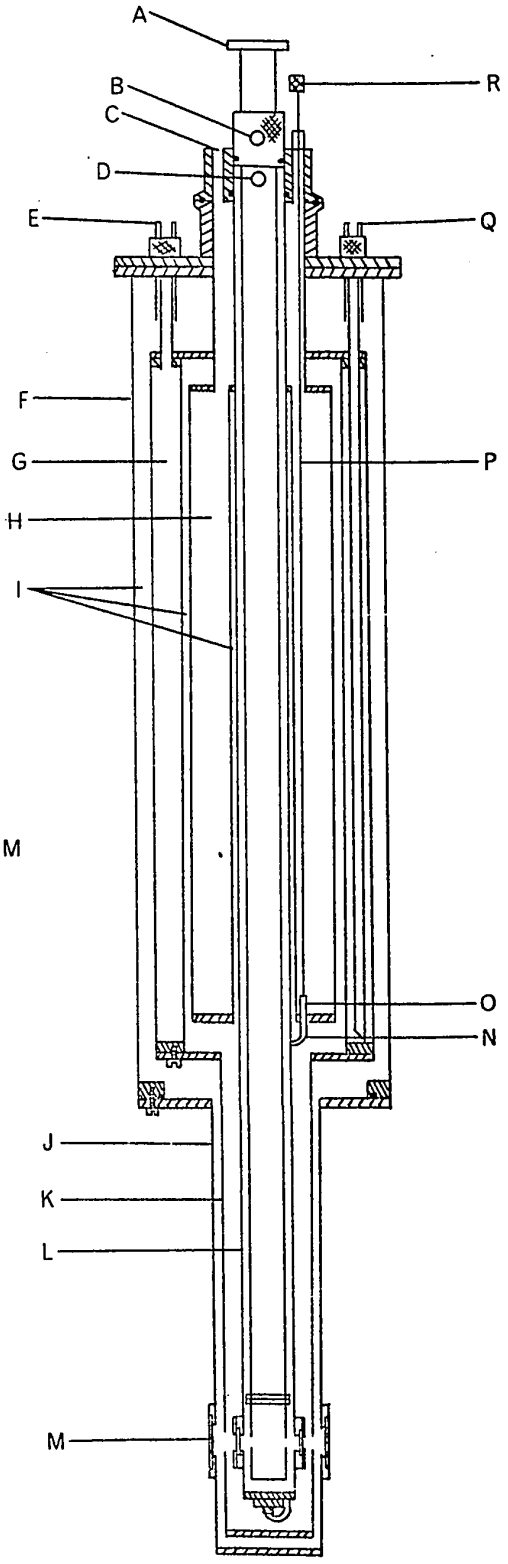

Fig. 11(a) The liquid helium cryostat

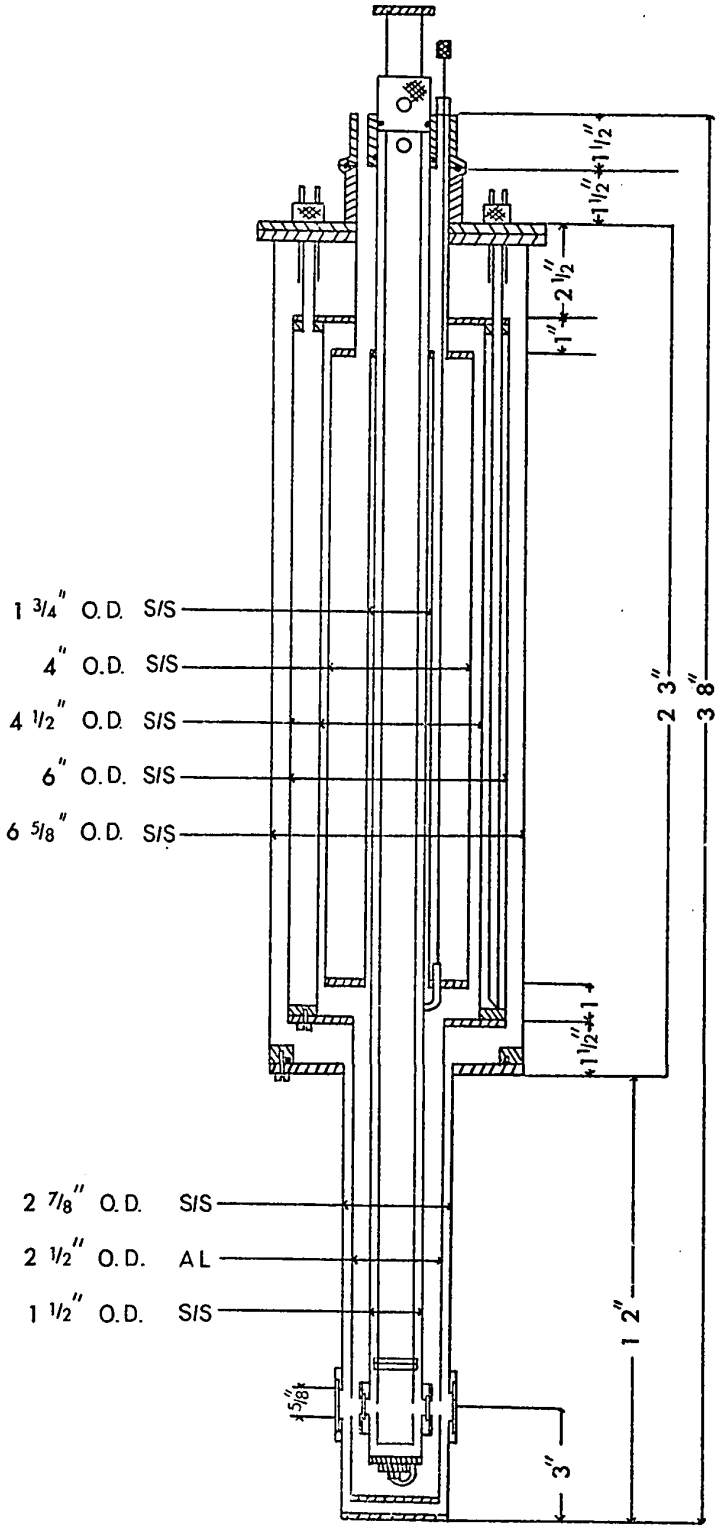

Fig. 11(b) The liquid helium cryostat

The top of the cryostat is equipped with an evacuation valve, helium pumping arm (D), electrical feedthrough (B), an ion gauge, and an access to the sample region.

The inner tail (L) or sample region provides the environment in which the experiment is performed. Helium flows from the helium reservoir (H) via a capillary tube (N) to the bottom of the tail and then is diffused by packed fibre-glass. The rate of flow of helium is controlled by the throttle valve (O). Brass flanges with half inch holes were brazed to the tail to hold 0.020 thick beryllium windows. It was hoped that an epoxy mixture compounded by weight of Epon 828 resin and Versamid 125 hardener [12] could be used but it was found that the epoxy mixture cracked after cooling and warming several times. The windows were then sealed by indium O-rings. The only drawback of using the indium seals is that indium becomes superconducting at a temperature of 3.41°K.[7] The critical value of the magnetic field for the destruction of superconductivity in indium is 280 G at a temperature of 1.5°K so that this effect should not hinder the experiment of interest.

The radiation shield (K) is constructed of highly polished aluminum with half inch holes for irradiation of the sample. The presence of these holes does not noticeably hamper the cooling of

the sample region. Aluminum is used rather than copper for the radiation shield because aluminum does not tarnish whereas copper does. At 77°K the thermal conductivity of aluminum is only slightly higher than that of copper and at 7°K the conductivity of aluminum is eleven times that of copper.[13] No seals or windows are required on this shield as there is a common vacuum on both sides of it.

The outer tail (J) is again equipped with brass flanges and beryllium windows epoxied to them using the method described above. Rubber O-rings would have been satisfactory here but it was necessary to keep the cross section of the tail within 3.125 inches. The outer tail is hermetically sealed to the outer shell (F) by rubber O-rings.

The cryostat has two vacuum systems: an oil diffusion pump to evacuate the insulation space (I) to a pressure of no greater than 10^{-4}mm of mercury and a high speed rotary pump to reduce the vapour pressure of the helium gas to obtain temperatures below 4.2°K.

4.1 Temperature Measurement and Control

The temperature controller is an Artronix model 5301. This instrument can control over a range of 1.0°K to 320°K with

six ranges for sensors with positive temperature coefficients, 1.0 ohms to 120.0 ohms and six ranges for sensors with negative temperature coefficients, 4.0 ohms to 15 k ohms. The temperature set control is a ten turn dial which provides continuous temperature settings throughout each range selected. This dial was calibrated using a standard resistance box and selecting the values of resistance from the temperature versus resistance curves for the germanium and platinum resistance thermometers (the resistance thermometers were calibrated by R. Krawczyniuk). Each curve of temperature set versus temperature was then fitted to a polynomial of maximum degree ten. The results are tabulated in Appendix B.

The germanium resistor was calibrated from 1.61°K to 37.11°K and the platinum resistor from 29.96°K to 102.40°K. The temperature is known to within 0.95 percent for the germanium resistor and 0.75 percent for the platinum resistor with respect to the calibration curve. For temperatures from 102.40°K to 294.61°K there were only several points to calibrate each range thus the error may be increased to 3.0 percent for these temperatures.

The two temperature sensors are mounted in the brass flange directly above the sample cavity. The temperature is

controlled by a 100 ohm double silked manganin heater wrapped around the bottom of the cavity. The heater is capable of producing up to 25 w rms. The power output has three ranges; low (1 watt), medium (5 watts) and high (25 watts). Each range is controlled by a ten turn dial which indicates the average power output of the controller. The controller can be operated manually for "start up" and then automatically at which time the heater is internally driven to provide the correct average power output as well as to reduce possible offset.

CHAPTER V

THE EXPERIMENTAL PROCEDURE

A paramagnetic resonance experiment was performed on d.p.p.h. and a single crystal of chromium potassium alum ($CrK(SO_4)_2 \cdot 12H_2O$) to demonstrate the operation of the spectrometer. An outline of a typical experiment will be given here; in particular the results for d.p.p.h. and ($CrK(SO_4)_2 \cdot 12H_2O$) will be discussed.

After the crystal to be investigated has been mounted in the centre of the cavity on the broad side, the cavity arm is placed inside the cryostat. The insulation space is then pumped down to a pressure of no greater than 10^{-4} mm. The sample region and the helium reservoir are purged with helium gas to prevent air from freezing in the capillary tube and in the sample region of the cryostat. The nitrogen reservoir is then filled resulting in a further decrease of pressure in the evacuation space and pre-cooling of the overall system.

The klystron power supply is switched on and the klystron frequency is tuned to the resonance frequency of the cavity with the reflector voltage modulated by a 60 Hz sinusoidal signal. The magnet, modulation field, automatic frequency control and lock-in-

amplifier are switched on and allowed one half hour to warm up. After the cryostat has been allowed to cool for four to five hours the helium is transferred from a 25 litre capacity storage container via a transfer tube to the helium reservoir by applying a small pressure to the container. Once the helium remains as a liquid in the reservoir the insulation vacuum decreases rapidly to better than 10^{-9} mm of mercury. Once cryopumping begins the cryostat is closed off from the oil diffusion pump.

After the transfer is complete, the rotary vacuum pump is turned on to slightly reduce the pressure in the sample region and the throttle valve is opened. The temperature control is first used to monitor the cooling. At the desired temperature the heater is turned on and the temperature controlled manually. When the temperature appears to be reasonably stable the controller is turned to the "automatic mode". It is important here that the stability is within .01°K as small changes in the temperature cause the cavity tuning and frequency to change.

The cavity is now tuned to the correct frequency and crystal leakage. The 60 Hz modulation is removed and the automatic frequency control is connected into the circuit. The magnetic field is then slowly increased until a resonance absorption is found.

The magnetic field is then set on a maxima of the derivative of the absorption curve plotted on the X-Y recorder. The frequency and phase of the signal channel of the lock-in-amplifier are tuned to 390 Hz, the frequency of the signal being reflected from the cavity. The time constant is adjusted for best signal to noise ratio and final adjustments are made to the microwave bridge to obtain the best representation of the absorption signal.

5.1 Diphenyl Picryl Hydrazl (d.p.p.h.)

The condition for resonant absorption is given by Eq. 2. For d.p.p.h., $g=2.0036 \pm 0.0002$.[14] Thus for a frequency of 9.46 gHz the resonant value of the dc magnetic field is 3373.43 gauss.

Figure 12 shows the derivative of absorption curve for a powdered sample of d.p.p.h. The center line is at 3373.51 gauss and the peak to peak line-width (ΔH_{pp}) is 0.85 gauss. The value of the parameter $A/y'_m (\Delta H_{pp})^2$ is 1.9, where y'_m is one half the peak to peak height and A is the area under the curve. A reported value of this parameter is 2.2.[5]

The line-width depends upon the number of spins present in the sample which for d.p.p.h. should be 6×10^{12}. This amounts to the mass of the sample being less than 4.0×10^{-9} grams. Although it is

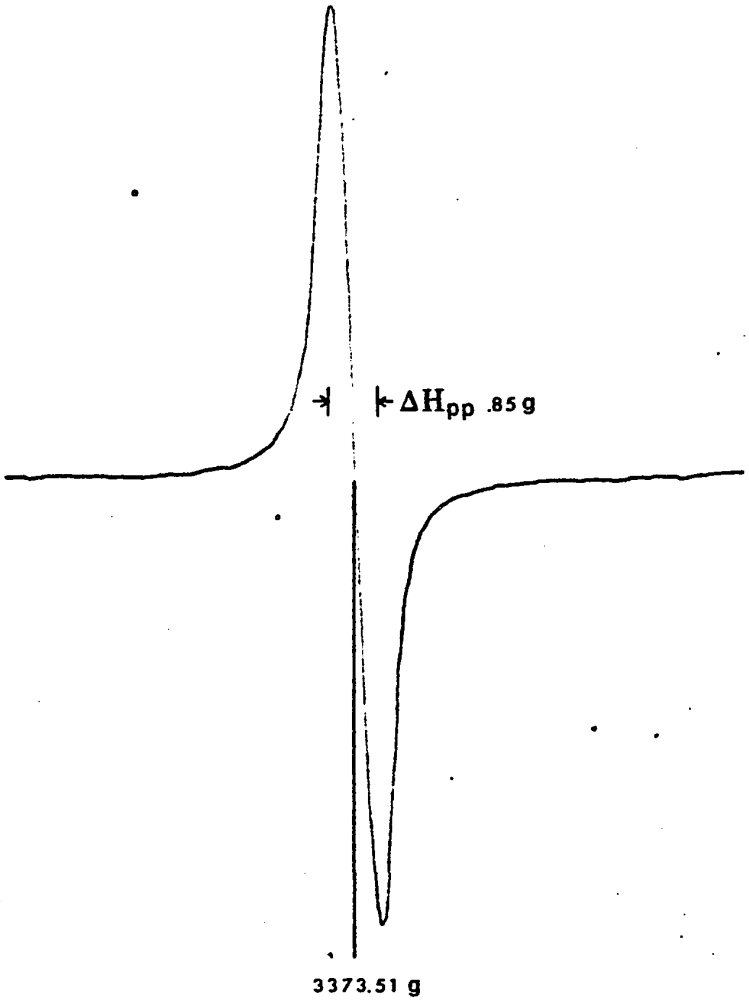

Fig. 12 Derivative of absorption curve for a powdered sample of d.p.p.h.

difficult to weigh the sample, the mass used was presumably greater than 4.0×10^{-9} grams. The second factor which contributes to the broadening of the line-width is the amplitude of the ac magnetic field. The modulation amplitude should be ten times less than the line-width in order to obtain the value 0.85 for ΔH_{pp}. This would require an extremely sensitive spectrometer. No attempt was made to measure the modulation amplitude. It should be noted that none of the two sources of broadening affect the centre position of the line.

5.2 Chromium Potassium Alum ($CrK(SO_4)_2 \cdot 12H_2O$)

Chromium potassium alum has been studied more extensively than perhaps any other substance and with more divergent results.[15] We made a full investigation of the salt by sweeping the magnetic field in two planes, (a) the plane perpendicular to the $(\bar{1}\bar{1}1)$ direction and (b) the plane perpendicular to the (001) direction. The discussion is made with particular attention to three orientations of the dc magnetic field, namely, in the directions perpendicular (a) to a {100} face, (b) to a {110} face, and (c) to a {111} face.

The crystal structure of this salt has been studied by X-ray diffraction methods[16], as well as optical goniometry.[17] The usual

form of the crystal is octahedral as shown in Fig 13, having faces $\{111\}$, $\{\bar{1}11\}$, $\{\bar{1}\bar{1}1\}$, $\{1\bar{1}1\}$, $\{11\bar{1}\}$, $\{\bar{1}1\bar{1}\}$, $\{\bar{1}\bar{1}\bar{1}\}$, and $\{1\bar{1}\bar{1}\}$. During early growth $\{100\}$ and $\{110\}$ faces form only to disappear later. None of our crystals showed $\{100\}$ or $\{110\}$ faces.

The unit cell, which is cubic, contains four inequivalent chromium ions, each subject to a crystalline electric field of predominately cubic symmetry. There is superimposed on this a small trigonal component whose axis of symmetry is directed along one of the body diagonals of the unit cube, the diagonals being different for each of the four ions. This trigonal component causes splitting of the otherwise quadruply degenerate ^4S state into two doublets. Furthermore, when a magnetic field is applied, the behaviour of the energy levels depends on the angle θ which the magnetic field makes with the trigonal axis. Thus the paramagnetic resonance spectrum which arises from transitions between these levels also depends on θ, and is specified by the parameter $c = \cos^2\theta$. It has been shown that the energy of a spin level is given by one of the roots of the equation[18]

$$W^4 + 2aW^3 + W^2(a^2 - 10\mu_0^2H^2) - 2aW\mu_0^2H^2(7 - 6c) + 9\mu_0^4H^4 - a\mu_0^2H^2(4 - 3c) = 0$$

in which a is the splitting parameter of the spin levels, μ_0 is the Bohr magneton, H is the magnetic field and W is the energy of a level.

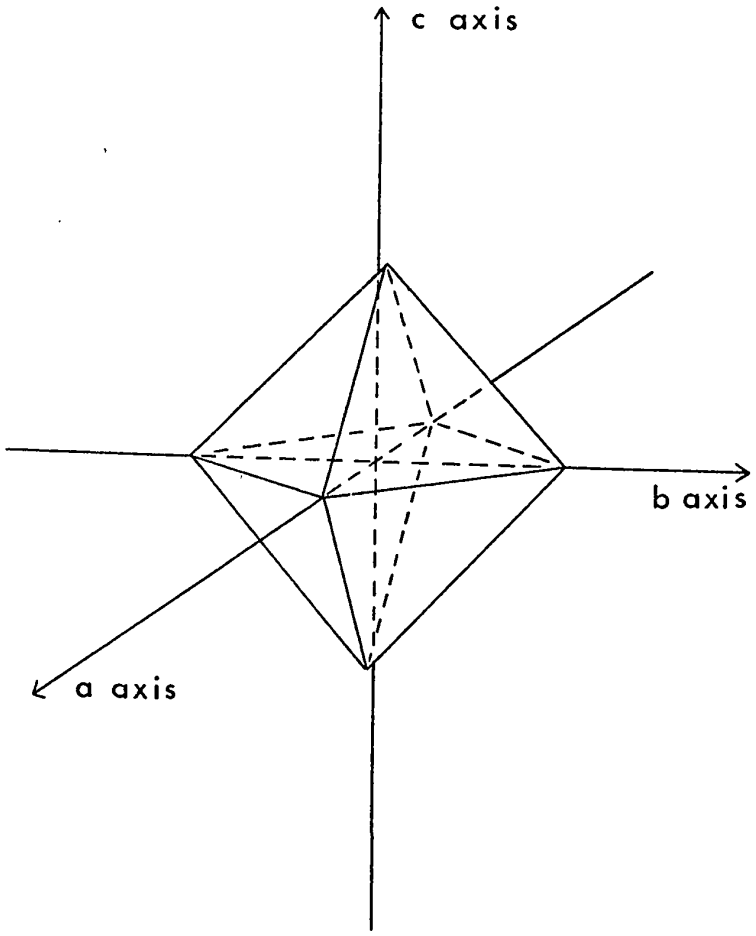

Fig. 13 Crystal habits of $CrK(SO_4)_2 \cdot 12H_2O$

In general, the four different ions give four superimposed spectra, but simple cases arise when the magnetic field is directed along the axis of the unit cube (001), or a body diagonal (111) axis. In the former case, the four ions give identical spectra; in the latter the magnetic field is parallel to the trigonal axis of one ion, for which case the behaviour of the energy levels is particularly simple as c = 1, and the above equation can be solved rigorously. The levels diverge linearly as the strength of the magnetic field and lie respectively at

$$W_1 = -a + (3/2)g\beta H$$

$$W_2 = (1/2)g\beta H$$

$$W_3 = -(1/2)g\beta H$$

$$W_4 = -a - (3/2)g\beta H$$

Since the allowed transitions involve changes of ± 1 in the magnetic quantum number (when the rf field is perpendicular to the dc magnetic field), the spectrum consists of a central line at $h\nu = g\beta H$, flanked by two equidistant satellities at $g\beta H \pm a$. Thus the central line gives the value of g, which will be close to 2 for a free electron spin, and the separation of the satellites gives the splitting parameter a.

Superimposed on this spectrum is that due to the other ions in the unit cell, for each of which $c = \cos^2\theta = 1/9$. The energy levels for this case, and therefore the spectrum, are fixed once the parameter a is known. The same is true when the magnetic field is applied in the (001) or any other direction.[19]

Figures 14 and 15 show the derivative of absorption curves at a frequency of 9.46 gHz of undiluted single crystals of $CrK(SO_4)_2 \cdot 12H_2O$ at room temperature. The position of the sharp peaks could be determined within ± 20 gauss but the error will be greater due to interference in amplitude and phase for several overlapping resonances. Figure 16 shows the angular variation of H in a plane perpendicular to the (001) direction. At 0° the magnetic field is perpendicular to the {110} face and at 45° the magnetic field is perpendicular to the {100} face. Figure 17 shows the values of H when the magnetic field is swept in a plane perpendicular to the $(\bar{1}\bar{1}1)$ direction. At 5° the magnetic field is perpendicular to the {111} face.

Table 3 gives a comparison of our results with those obtained by Whitmer, Weinder, Hsiang and Weiss.[20] The first two columns are their calculated and experimental data and the third is our experimental data. The fourth column is data obtained by Ting and Williams.[21] The table shows reasonable agreement with the published data.

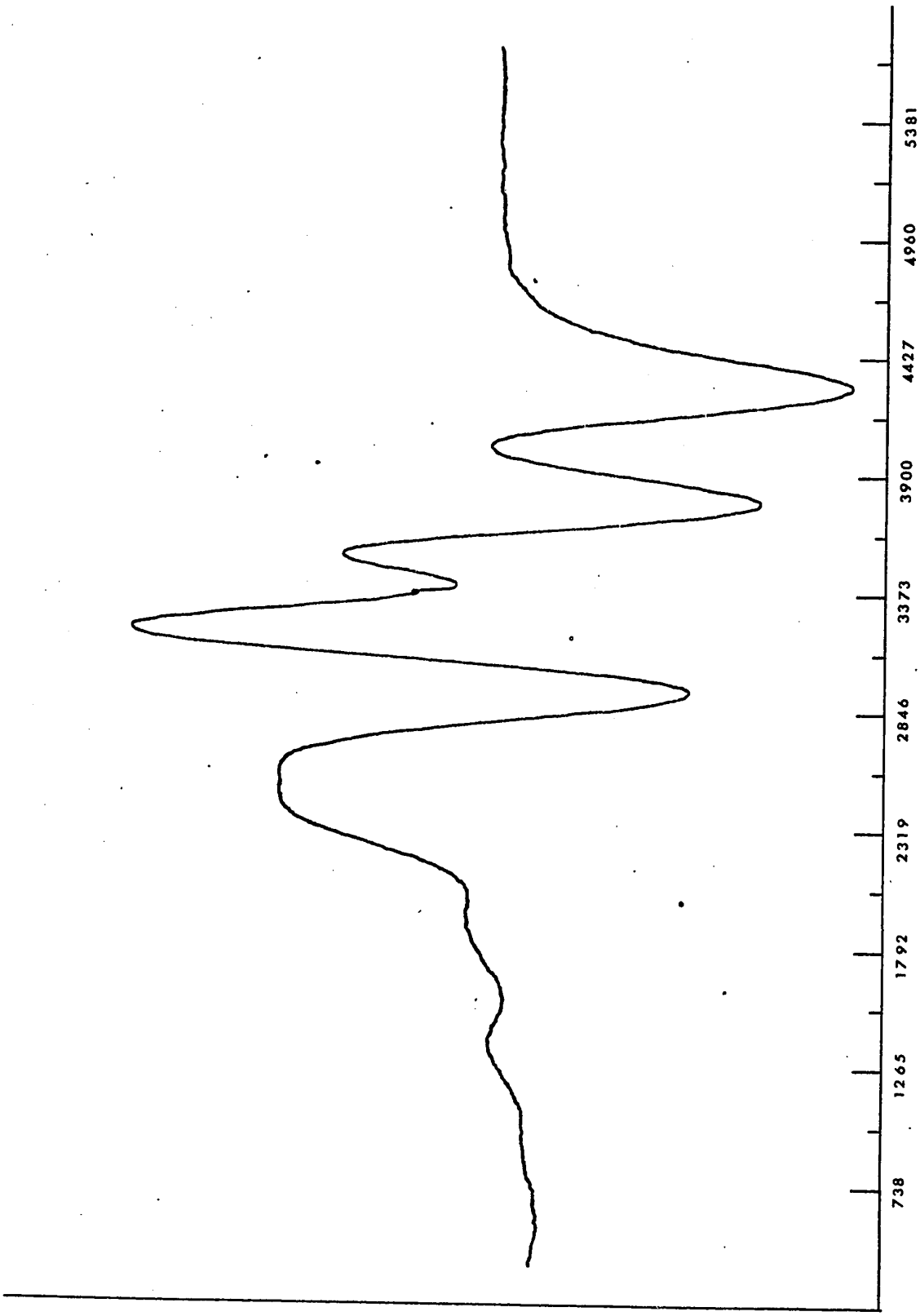

Fig. 14 Derivative of absorption curve of $CrK(SO_4)_2 \cdot 12H_2O$ with $H \perp$ the (110) face

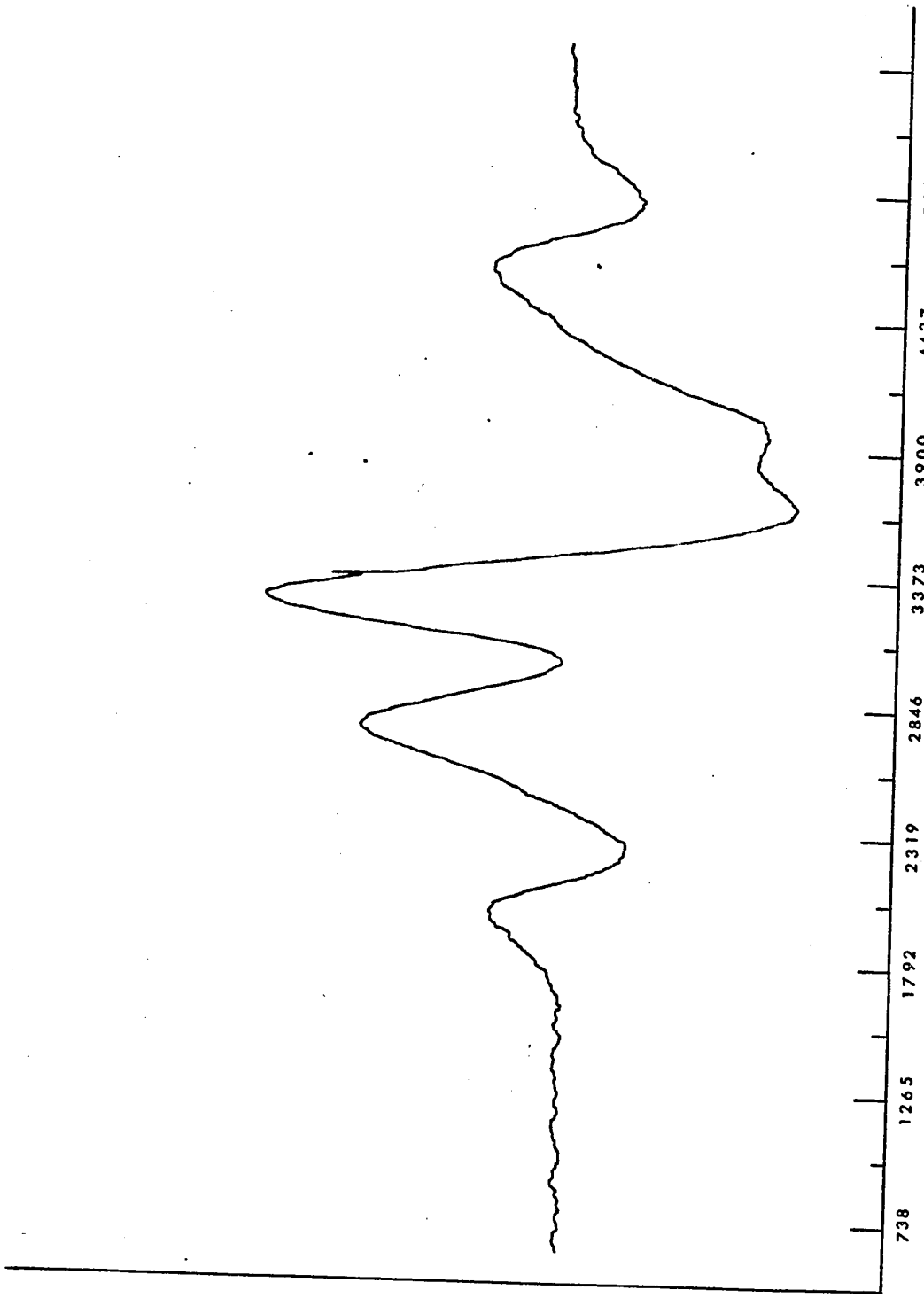

Fig. 15 Derivative of absorption curve of $CrK(SO_4)_2 \cdot 12H_2O$ with $H \perp$ the (111) face

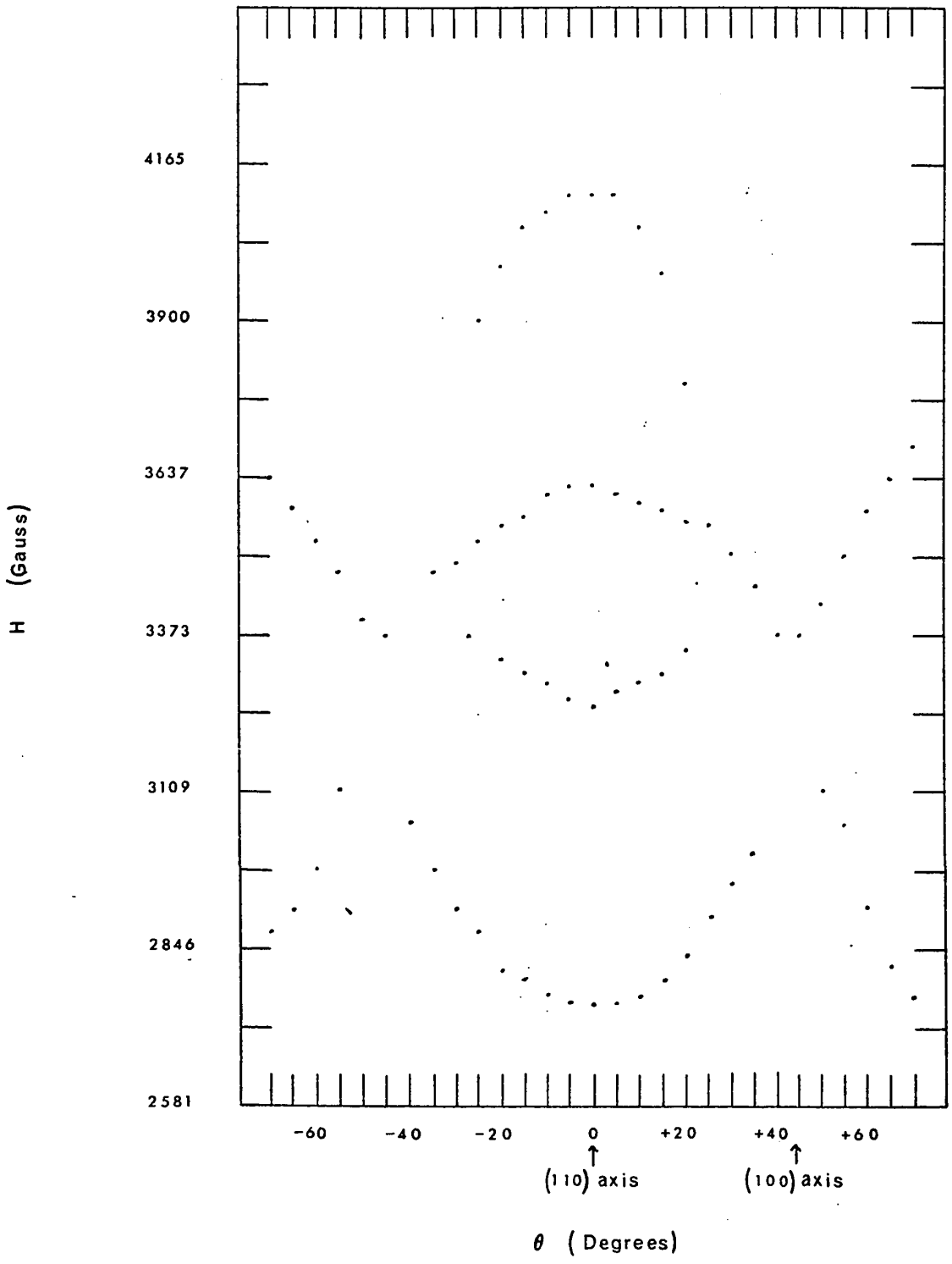

Fig. 16 Angular variation of H in a plane perpendicular to the (001) direction

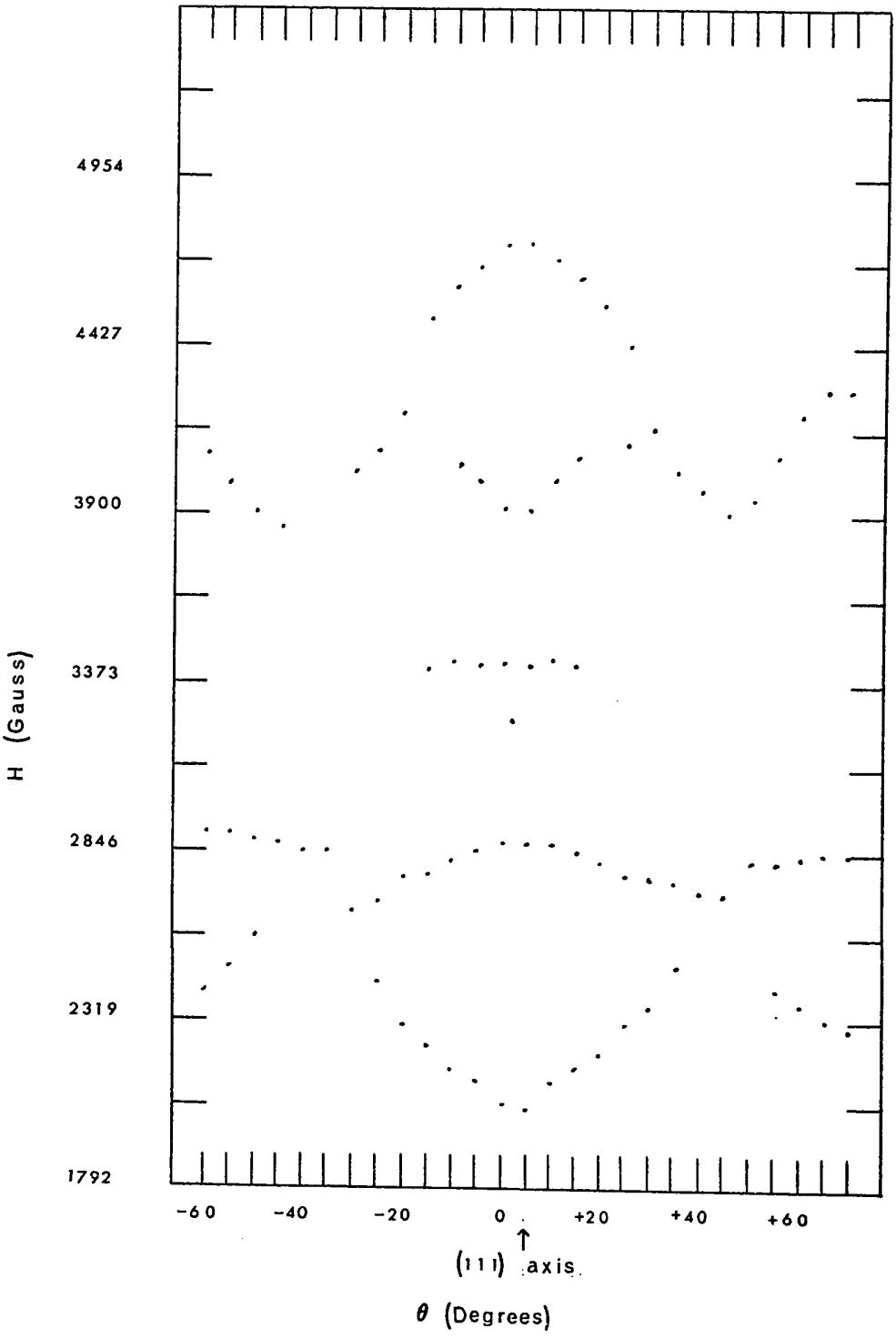

Fig. 17 Angular variation of H in a plane perpendicular to the $(\bar{1}\bar{1}1)$ direction

Table 3 Observed and calculated magnetic field values of absorption maxima for $CrK(SO_4)_2 \cdot 12H_2O$ at T = 295°K

Direction	Calc.	Exp.	Exp.	Exp.
	2008	2008	2108	
	2865	2825	2872	
(111)	3400	3400	3438	
	3783	*	3966	
	4802	4802	4730	
	2522	2522	*	*
(110)	2754	*	2743	2693
	3309	3269	3268	3260
	3581	3632	3623	3538
	3884	*	*	*
	4106	4167	4114	4135
	3198			
(100)		3289	3373	
	3551			

Figure 18 shows the derivative of absorption curve of $CrK(SO_4)_2 \cdot 12H_2O$ at 1.92°K. This temperature is achieved by lowering the vapour pressure of the helium in the sample region of the cryostat by pumping. According to Bleaney,[19] as one lowers the temperature starting from room temperature, $CrK(SO_4)_2 \cdot 12H_2O$

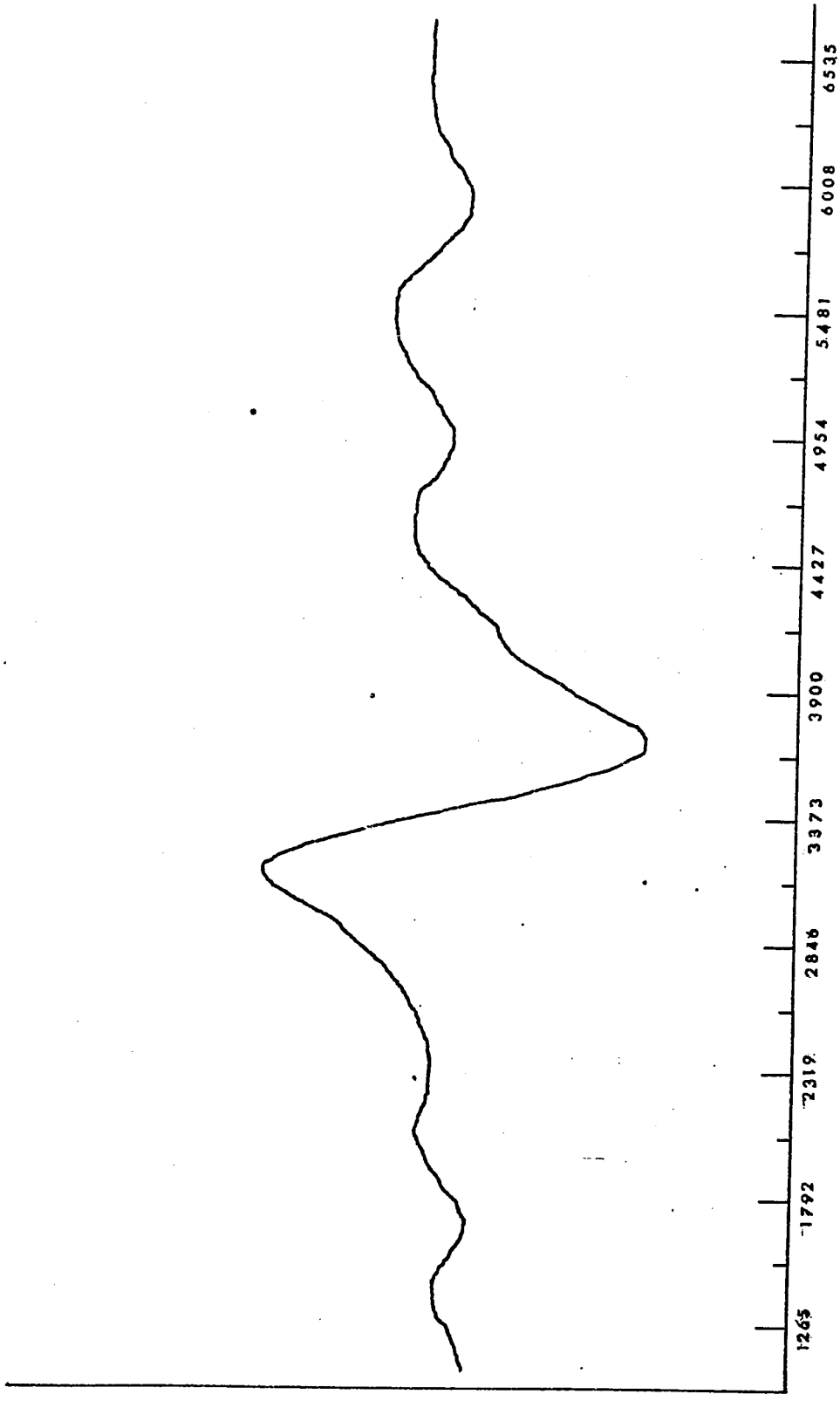

Fig. 18 Derivative of absorption curve of $CrK(SO_4)_2 \cdot 12H_2O$ with H⊥the (111) face

undergoes a phase transition at 160°K. The stress of the phase transition shatters the crystal into micro-crystals which would presumably have parallel axes. The paramagnetic resonance spectrum indicates that below the transition temperature this alum must have a different crystal structure.

Table 4 Observed magnetic field values of absorption maxima for $CrK(SO_4)_2 \cdot 12H_2O$ at 1.92°K

Direction	Exp.	Exp.
	5719	5636
	4665	4549
(111)	3399	3437
	2292	2350
	1501	1592

The position of our five lines at 1.92°K are compared in Table 4 (column 1) with those obtained by Halliday and Wheatley[22] (column 2) at 90°K (no measurements have been reported in the literature at 1.92°K). The two sets of results agree reasonably well. The position of the peaks would be expected to remain unchanged at temperatures below the transition temperature, althouth the intensities of the lines may change due to different populations of the levels at different temperatures.

CHAPTER VI

CONCLUSION

An X-band paramagnetic resonance spectrometer and a low temperature cryostat, suitable for the detection of dynamically oriented nuclei by the Mössbauer effect are constructed. In particular an automatic frequency control unit for the klystron unit has been assembled. The cryostat is suitable for experiments at liquid helium temperatures and has provision for transmitted gamma-rays to irradiate a sample place inside it.

The overall performance of the spectrometer has been demonstrated by obtaining e.p.r. spectra of two samples, namely, diphenyl picryl hydrazl and chromium potassium alum. The results obtained show satisfactory agreement with the published data.

Appendix A

Magnetic Field Calibration

Dial Field (gauss)	NMR Field (gauss)	Estimated Field	Percent Difference
1000.0	1004.8	1006.9	0.20
1400.0	1402.9	1402.7	0.01
1800.0	1798.8	1798.4	0.02
2200.0	2193.1	2194.2	0.05
2600.0	2588.6	2590.0	0.05
3000.0	2983.4	2985.8	0.03
3400.0	3379.9	3381.6	0.05
3800.0	3775.1	3777.4	0.06
4200.0	4169.6	4173.2	0.08
4600.0	4565.5	4568.9	0.07
5000.0	4965.5	4964.7	0.01
5400.0	5359.0	5360.5	0.02
5800.0	5756.0	5756.3	0.00
6200.0	6158.0	6152.1	0.09
6600.0	6549.4	6547.9	0.02
7000.0	6942.6	6943.7	0.01
7400.0	7340.0	7339.5	0.01
7800.0	7735.7	7735.2	0.00
8200.0	8135.7	8131.0	0.05
8600.0	8525.4	8526.8	0.01
9000.0	8921.9	8922.6	0.00
9400.0	9315.4	9318.4	0.03
9800.0	9710.7	9714.2	0.03

Appendix B

Thermometer Calibration

Germanium Range 2

Resistance	Temperature Set	Actual Temperature °K	Estimated Temperature °K	Percent Difference
269.33	13.0	1.61	1.61	0.00
247.10	49.0	1.71	1.72	0.58
220.41	100.0	1.88	1.88	0.00
197.66	152.0	2.09	2.09	0.95
175.42	211.0	2.35	2.37	0.84
148.61	299.0	2.71	2.73	0.73
133.57	359.0	3.03	3.03	0.00
116.35	438.0	3.44	3.43	0.29
101.00	522.0	3.88	3.86	0.51
88.99	600.0	4.26	4.28	0.46
79.34	672.0	4.69	4.71	0.42
71.86	734.0	5.15	5.12	0.58
59.89	847.0	5.95	5.96	0.16
49.54	965.0	6.86	6.86	0.00

Germanium Range 3

88.99	41.0	4.26	4.26	0.00
79.34	122.0	4.69	4.70	0.21
71.86	192.0	5.15	5.14	0.19
59.89	325.0	5.95	5.96	0.16
49.54	468.0	6.86	6.85	0.14
37.99	666.0	8.18	8.18	0.00
31.64	802.0	9.36	9.36	0.00
26.63	923.0	11.78	11.78	0.00
24.71	974.0	13.84	13.84	0.00

Germanium Range 4

31.64	47.0	9.36	9.36	0.00
25.53	218.0	11.78	11.79	0.08
24.71	290.0	13.85	13.81	0.28
22.90	364.0	16.21	16.25	0.24
22.09	397.0	17.28	17.30	0.11
20.29	478.0	20.07	20.03	0.23
19.58	510.0	21.35	21.26	0.42
18.28	574.0	23.84	24.02	0.75
16.77	651.0	27.71	27.54	0.61
15.86	699.0	29.98	30.02	0.13
15.37	727.0	31.94	32.08	0.43
14.96	750.0	34.72	34.56	0.46
14.66	767.0	37.11	37.16	0.10

Platinum Range 1

4.42	340.0	29.98	30.10	0.40
4.92	370.0	31.94	31.76	0.56
5.52	406.0	34.72	34.52	0.57
6.32	450.0	37.11	37.34	0.61
7.13	492.0	42.06	41.99	0.16
8.34	552.0	45.70	45.76	0.13
9.64	611.0	49.72	49.66	0.12
11.05	670.0	53.31	53.48	0.31
12.76	734.0	57.92	57.88	0.06
15.16	819.0	64.50	64.44	0.09
18.68	920.0	73.31	73.36	0.05

Platinum Range 2

20.79	108.0	78.94	78.96	0.02
22.40	199.0	82.62	82.57	0.06
25.52	360.0	89.72	89.80	0.08
27.63	458.0	94.93	94.87	0.06
30.65	586.0	102.41	102.41	0.00

BIBLIOGRAPHY

1. E. Zavoisky, J. Phys. (U.S.S.R.) 41, 211 (1945).
2. B. Bleaney and R.P. Penrose, Nature 157, 339 (1946).
3. S.K. Misra and W.A. Barker, Phys. Rev., 138, A58 (1965).
4. S.K. Misra and J.M. Daniels, Can. J. Phys., 43, 1843 (1965).
5. C.P. Poole, Electron Spin Resonance, John Wiley and Sons, New York (1967).
6. A. Abragam and B. Bleaney, Electron Paramagnetic Resonance of Transition Ions, Clarendon Press, Oxford (1970).
7. C. Kittel, Introduction to Solid State Physics, John Wiley and Sons, New York (1953).
8. G. Feher, Bell System Tech. J., 36, 449 (1957).
9. A.E. Booth, Microwave Data Tables, Iliffe and Sons, London (1959).
10. R.S. Alger, Electron Paramagnetic Resonance, John Wiley and Sons, New York (1968).
11. J.M. Daniels and H.A. Farach, Rev. Sci. Instr. 32, 1262 (1961).
12. C.J. Rauch and W.C. Kernon, Rev. Sci. Instr. 33, 496 (1962).
13. W.M. Zemansky, Heat and Thermodynamics, McGraw Hill, New York (1957).

14. A.N. Holden, C. Kittel, F.R. Merritt, and W.A. Yager, Phys. Rev. 77, 147 (1950).

15. J.M. Daniels, Oriented Nuclei, Academic Press, New York (1965).

16. C.A. Beevers and H. Lipson, Proc. Roy. Soc. A, 146, 570 (1934).

17. R. Groth, Chem. Krystallog., 2, 565 (1908).

18. L.J.F. Broer, Physica, 9, 547 (1942).

19. B. Bleaney, Proc. Roy. Soc. A, 204, 203 (1950).

20. C.A. Whitmer, R.T. Weidner, J.S. Hsiang, and P.R. Weiss, Phys. Rev., 74, 1478 (1948).

21. Y. Ting and D. Williams, Phys. Rev., 82, 507 (1951).

22. D. Halliday and J. Wheatley, Phys.Rev., 74, 1712 (1948)